Journal of Quantitative Spectroscopy & Radiative Transfer 246 (2020) 106924

Contents lists available at ScienceDirect

Journal of Quantitative Spectroscopy & Radiative Transfer

journal homepage: www.elsevier.com/locate/jqsrt

Revisiting independent versus dependent scattering regimes in suspensions or aggregates of spherical particles

Tiphaine Galy, Daniel Huang, Laurent Pilon*

Mechanical and Aerospace Engineering Department, Henry Samueli School of Engineering and Applied Science, University of California, Los Angeles, USA

ARTICLE INFO

Article history:
Received 26 November 2019
Revised 5 February 2020
Accepted 21 February 2020
Available online 22 February 2020

Keywords:
Light scattering
Lorenz-Mie theory
Multiple scattering
Interference
Interaction

ABSTRACT

Independent scattering refers to situations when particles are sufficiently distant that some of the radiation characteristics of particle systems can be determined by adding the contributions of each particle. When particles are in close proximity, however, dependent scattering prevails and is affected by near-field interactions and far-field interferences among scattered waves from nearby particles. The dimensionless parameters governing the scattering cross-section and asymmetry factor of non-absorbing bispheres, disordered and ordered suspensions and aggregates with up to 8 spherical particles were found to be the particle size parameter χ_s, the relative index of refraction m, the interparticle distance-to-wavelength ratio d^*, and the number of particles. Here, χ_s ranged from 0.031 to 8.05, m varied from 0.667 to 2.6, and d^* reached up to 30. Dependent effects were observed in aggregates with particles of all sizes and were strongly affected by the relative index of refraction in particle systems with $\chi_s \geq 2$ due to large phase shifts across the particles. Moreover, new criteria for the transition between the dependent and independent scattering regimes for the scattering cross-section and the asymmetry factor were derived. For the scattering cross-section of structures with a narrow interparticle distance distribution, the independent scattering regime prevailed when the average interparticle distance-to-wavelength ratio $\bar{d}^*$ exceeded (i) 2 for particles with $\chi_s \leq 2$ and (ii) 5 for particles with $\chi_s > 2$. For the asymmetry factor, the transition from the dependent to the independent regimes for particles with $\chi_s \leq 2$ was achieved for $\bar{d}^*$ as high as 25. These transition criteria could be extended to particle systems with a broad interparticle distance distribution when based on the minimum interparticle distance-to-wavelength ratio. Finally, the relative index of refraction m did not affect these transition criteria.

1. Introduction

Electromagnetic wave scattering by suspensions and aggregates of spherical particles is of interest to a wide range of applications. Fig. 1 presents micrographs of carbon aerosols from combustion systems [1], silica aerogels for thermally insulating windows [2], suspensions of nickel nanoparticles used in solar to thermal energy conversion [3], and disperse titania particles used in paints and coatings [4]. In all these applications, the incident radiation is unpolarized and its transport through the particulate media is governed by the radiative transfer equation (RTE). Then, knowledge of the integral radiation characteristics of the particle suspensions or aggregates namely their absorption and scattering cross-sections and asymmetry factor is of prime importance to predict the local radiation intensity by solving the RTE. In fact, the scattering characteristics of atmospheric aerosols with particle size ranging from 0.1 to 5 μm, such as carbon aerosols [Fig. 1(a)], have been studied from the near ultraviolet (UV) to the near infrared (IR) to determine their effect on the Earth climate [5,6]. Furthermore, transparent monoliths of silica aerogels, consisting of a highly porous network of silica nanoparticles [Fig. 1(b)] with radius $r_s \leq 20$ nm, have been used in solar collectors [7] and for thermal insulation in window applications [8]. The optical clarity and haziness of silica aerogel slabs depend on their scattering characteristics in the visible [9]. Similarly, the efficiency of nanofluid-based solar collectors depends on the scattering characteristics of the nanoparticle suspension [Fig. 1(c)] with radius $r_s < 50$ nm from the near UV to the near IR [3,10,11]. Finally, the visual appearance of particle-based paints and coatings under visible light depends on the scattering characteristics of the particle systems [12,13]. Titania particles [Fig. 1(d)] featuring sizes ranging from tens to hundreds of nanometers are commonly used in paints or coatings to achieve whiteness and opacity [12].

The scattering cross-section and asymmetry factor of particle suspensions are typically determined by assuming that the particles scatter independently from one another so their individual

* Corresponding author.
E-mail address: pilon@seas.ucla.edu (L. Pilon).

https://doi.org/10.1016/j.jqsrt.2020.106924
0022-4073/

Nomenclature

C_{abs}	absorption cross-section, nm^2
C_{sca}	scattering cross-section, nm^2
c	clearance distance, nm
$\bar{c}$	average clearance distance, nm
d	interparticle distance, nm
$\bar{d}$	average interparticle distance, nm
$d_{\min}$	minimum interparticle distance, nm
c^*	clearance-to-wavelength ratio, $c^* = c/\lambda$
$\bar{c}^*$	average clearance-to-wavelength ratio, $\bar{c}^* = \bar{c}/\lambda$
d^*	interparticle distance-to-wavelength ratio, $d^* = d/\lambda$
$\bar{d}^*$	average interparticle distance-to-wavelength ratio, $\bar{d}^* = \bar{d}/\lambda$
$d^*_{\min}$	minimum interparticle distance-to-wavelength ratio, $d^*_{\min} = d_{\min}/\lambda$
c/r_s	clearance-to-radius ratio
d/r_s	interparticle distance-to-radius ratio
f_v	particle volume fraction
g	asymmetry factor
k_s	absorption index of particles
L	particles domain size, nm
m	relative complex index of refraction, $m = m_s/n_m$
m_s	particle complex index of refraction, $m_s = n_s + ik_s$
N_d	number of dipoles
N_s	total number of particles
n_m	refractive index of the surrounding medium
n_s	index of refraction of particles
Q_{sca}	scattering efficiency factor
r_{eq}	equivalent radius, nm
r_s	particle radius, nm
V_s	volume occupied by the particles, nm^3
V_{tot}	volume embedding the suspension/ aggregate, nm^3

Greek symbols

β	phase shift
χ_s	particle size parameter
Δd	dipole size, nm
λ	wavelength, nm
Φ	phase function
Ω	solid angle, sr
Θ	scattering angle, rad

Supercripts and subscripts

b	refers to bispheres
cr	refers to critical values delimiting the scattering regimes
M	refers to Lorenz-Mie theory
R	refers to Rayleigh scattering
s	as a superscript: refers to particle suspensions or aggregates

contributions can be added, based on superposition principles [14]. The validity of this approximation, sometimes called "independent scattering approximation" [14,15], depends on some measure of the proximity of the constitutive particles such as the particle volume fraction [15–18], the interparticle distance [6,16,18,19], and/or the particle surface-to-surface (or clearance) distance [15,17,20]. In situations when the particles are spherical, the Lorenz-Mie theory can be used to predict the scattering cross-section and asymmetry factor of each individual particle [21]. The independent scattering approximation has been used to determine the size distribution and concentration of atmospheric aerosols from measurements of their phase functions performed in the visible [22,23]. Furthermore, it has also been used to model the scattering cross-section of nanofluid-based absorbers for solar collectors [3,10,11]. Recently, Mishchenko [24] refined the definition of the independent scattering regime as the situation when "certain optical observables (i.e., appropriately defined second moments in the electromagnetic field) for the entire group can be expressed (explicitly or implicitly) in appropriate single-particle observables".

Conversely, "dependent scattering" refers to the situation when a scattering characteristic of particle systems cannot be determined by merely adding up the contributions of individual particles [14,15]. Mishchenko [24] established that the so-called first-order-scattering approximation for sparsely distributed particles and the radiative transfer theory for a cloud of particles "may be the only notable manifestations of the independent scattering regime, all other electromagnetic scattering by particulate media belonging to the category of dependent scattering". Moreover, dependent effects can change the energy budget of the particle system and the local radiation intensity [12,25]. Several criteria for the transition between the independent and dependent scattering regimes of bispheres, suspensions and aggregates of spherical particles have been proposed [6,15–18,20]. However, these criteria were (i) expressed using different parameters, (ii) derived for a limited range of values, and (iii) often disagreed with one another.

This study aims to unequivocally identify (1) the parameters controlling the scattering cross-section and asymmetry factor of bispheres, suspensions, and aggregates of non-absorbing monodisperse spherical particles and (2) the conditions under which independent and dependent scattering regimes prevail for the scattering cross-section and asymmetry factor of particle systems containing 2, 4, or 8 particles. A wide range of particle radius, wavelength, spatial configuration, and index of refraction were investigated.

2. Background

2.1. Light scattering by a single spherical particle

Scattering by a single spherical particle depends on its (i) size parameter χ_s and (ii) relative complex index of refraction m [14]. The particle size parameter χ_s is defined as $\chi_s = 2\pi r_s/\lambda$ where r_s is the particle radius and λ is the wavelength of the incident light. The relative complex index of refraction m is defined as $m = m_s/n_m$ where n_m is the index of refraction of the non-absorbing surrounding medium and m_s is the complex index of refraction of the particle defined as $m_s = n_s + ik_s$ where n_s and k_s are the refractive and absorption indices of the particle, respectively.

The scattering cross-section $C_{sca}(\chi_s, m, r_s)$ and asymmetry factor $g(\chi_s, m)$ of a single spherical particle in a non-absorbing medium can be predicted by the Lorenz-Mie theory [21]. Notably, in the Rayleigh scattering regime, corresponding to $\chi_s \ll 1$ and $\chi_s|m-1| \ll 1$, the scattering cross-section of a particle with size parameter χ_s and relative complex index of refraction m can be expressed as [26]

$$C^R_{sca}(\chi_s, m, r_s) = \frac{24\pi^3 V_s^2}{\lambda^4}\left|\frac{m^2-1}{m^2+2}\right|^2 = \frac{8\pi r_s^2 \chi_s^4}{3}\left|\frac{m^2-1}{m^2+2}\right|^2 \quad (1)$$

where V_s is the volume of the particle. On the other hand, the asymmetry factor g can be defined as [14]

$$g(\chi_s, m) = \frac{1}{4\pi}\int_{4\pi} \Phi(\chi_s, m, \Theta)\cos\Theta \mathrm{d}\Omega \quad (2)$$

where $\Phi(\chi_s, m, \Theta)$ is the scattering phase function representing the probability that a wave be scattered from the incident direction $\hat{s}_i$ into direction $\hat{s}$. Here, Θ is the scattering angle between unit vectors $\hat{s}_i$ and $\hat{s}$ and Ω is the associated solid angle. Particles in the Rayleigh scattering regime feature a negligible phase shift $\beta = 2\chi_s|m-1|$ between the incident electromagnetic wave and that

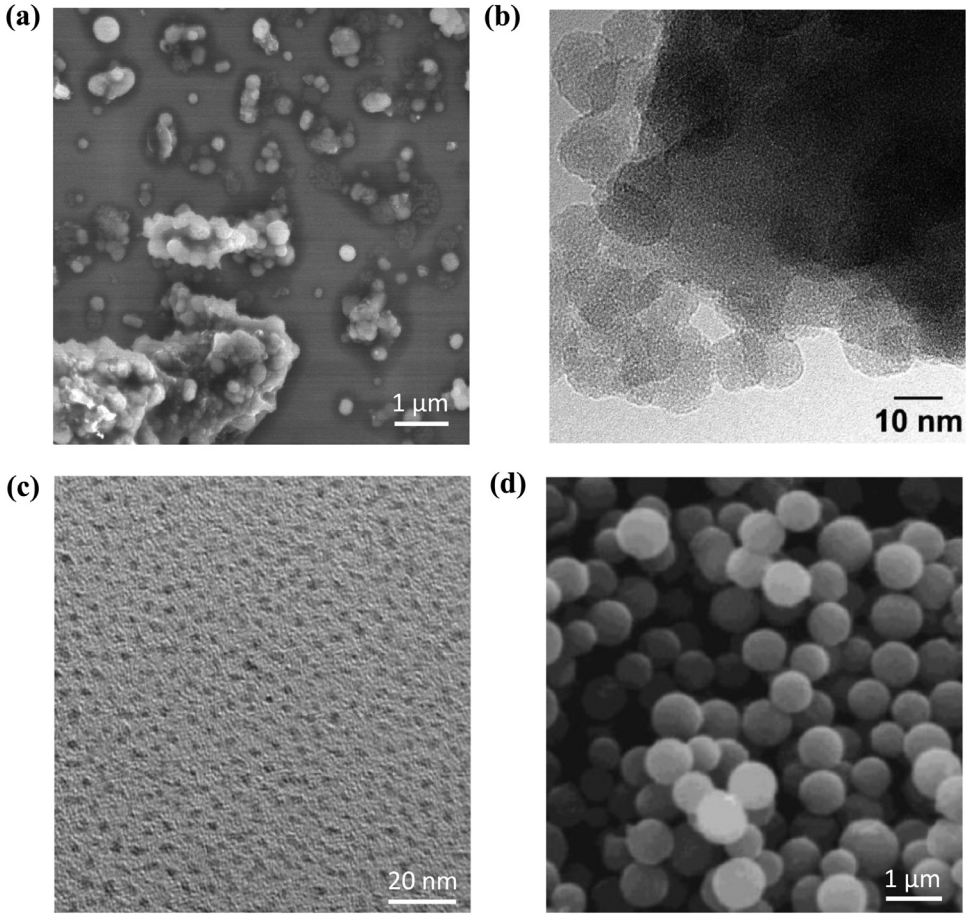

Fig. 1. Scanning electron microscopy images of (a) aerosol carbon particles (reprinted with permission from Ref. [1], Copyright Taylor & Francis) and (b) silica aerogel (reprinted with permission from Ref. [2]., Copyright Springer Nature). (c) Transmission electron image of nickel nanoparticle suspension (reprinted with permission from Ref. [3]., Copyright Elsevier) and (d) scanning electron image of titania particles (reprinted with permission from Ref. [4], Copyright John Wiley & Sons).

traveling through them [26,27]. Thus, their scattering phase function is isotropic, i.e., $\Phi(\chi_s, m, \Theta) \simeq 1$ and $g(\chi_s, m) \simeq 0$.

2.2. Light scattering by spherical particle suspensions and aggregates

Light scattering characteristics of a suspension or aggregate of spherical particles have been reported to depend not only on the particle (i) size parameter χ_s and (ii) relative complex index of refraction m but also on (iii) the particle volume fraction f_v of the suspension or aggregate [15–18], (iv) the average clearance-to-wavelength ratio $\bar{c}^* = \bar{c}/\lambda$ where $\bar{c}$ is the average surface-to-surface distance (or clearance distance) between adjacent particles [Fig. 2(a)] [15,17], (v) the average interparticle distance-to-wavelength ratio $\bar{d}^* = \bar{d}/\lambda$ where the average interparticle distance $\bar{d}$ is expressed as $\bar{d} = \bar{c}+2r_s$ [18,19], (vi) the average clearance-to-radius ratio $\bar{c}/r_s$ [15,20], and/or (vii) the average interparticle distance-to-radius ratio $\bar{d}/r_s$ [6,16]. The particle volume fraction f_v can be calculated as the ratio of the volume V_s occupied by the particles to the total volume V_{tot} of the suspension. For systems with monodisperse particles of radius r_s, f_v can be expressed as

$$f_v = \frac{V_s}{V_{tot}} \quad \text{with} \quad V_s = 4\pi r_s^3 N_s/3 \tag{3}$$

where N_s is the total number of particles in the total volume V_{tot} of the suspension.

When the particle volume fraction f_v is sufficiently low, particles are far from each other and the scattering characteristics of a particle are said to be "unaffected" by the presence of the surrounding particles corresponding to the independent scattering regime [14,15]. For example, in the independent scattering regime, the effective scattering cross-section C_{sca}^s of the suspensions can be expressed as the sum of the scattering cross-sections $C_{sca}(\chi_{s,i}, m_i, r_{s,i})$ of individual particles, i.e., [14]

$$C_{sca}^s = \sum_{i=1}^{N_s} C_{sca}(\chi_{s,i}, m_i, r_{s,i}). \tag{4}$$

Here, the index "i" corresponds to the particle of radius $r_{s,i}$ with size parameter $\chi_{s,i} = 2\pi r_{s,i}/\lambda$ and relative complex index of refraction m_i. Similarly, the asymmetry factor g^s of the suspension can be expressed as [28,29]

$$g^s = \frac{\sum_{i=1}^{N_s} C_{sca}(\chi_{s,i}, m_i, r_{s,i}) g(\chi_{s,i}, m_i)}{\sum_{i=1}^{N_s} C_{sca}(\chi_{s,i}, m_i, r_{s,i})} \tag{5}$$

where $g(\chi_{s,i}, m_i)$ is the asymmetry factor of the i^{th} particle. Note that for suspensions of identical monodisperse particles with size parameter χ_s and relative complex index of refraction m, Eqs. (4) and (5) simplify to $C_{sca}^s = N_s\, C_{sca}(\chi_s, m, r_s)$ and $g^s = g(\chi_s, m)$, respectively.

When particles are in close proximity, light scattering is affected by (i) near-field interactions and (ii) far-field interferences [6,28,30]. Near-field interactions originate from multiple scattering corresponding to the situation when the near-field scattered wave from one particle is incident on another particle leading, in turn, to interferences [6,28,30]. Far-field interferences refer to interferences between far-field-scattered waves from neighboring particles

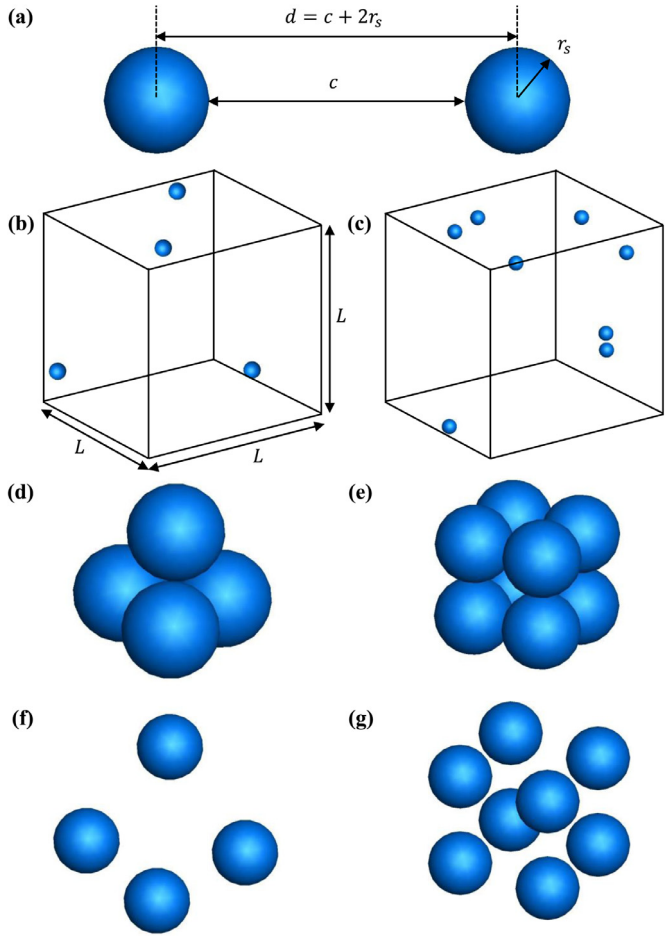

Fig. 2. Schematics of (a) bisphere, (b)-(c) disordered particle suspensions with N_s = 4 and N_s = 8, (d) tetrahedron and (e) simple cubic structure with touching particles, and (f) tetrahedron and (g) simple cubic structure with distant particles.

[6,28,30]. These two phenomena play an important role in the dependent scattering regime such that Eqs. (4) and (5) are no longer valid [14].

Previously, experiments or analytical derivations have been used to establish the range of validity of the independent scattering approximation. More recently, numerical algorithms solving Maxwell's equations in complex particulate media have been developed including the discrete dipole approximation (DDA) [31] and the superposition T-matrix method [32,33]. They have notably been used to analyze the range of applicability of the independent scattering approximation for radiative characteristics such as integral properties, scattering phase function, or scattering matrix elements [25].

2.3. Independent versus dependent scattering

Previous studies have investigated the independent and dependent scattering regimes in monodisperse bispheres [6,16,19,20,28], suspensions of spherical particles [15,17,18], or aggregates [15,17,20,34,35] based on experimental measurements [15,17], analytical derivations [15,19,28], or computer simulations [6,16,18,20,34,35]. In general, the independent scattering regime was considered to be reached when the radiation characteristic investigated (e.g., C^s_{sca} or g^s) of the particle system fell within 5% of the independent scattering regime predictions [Eqs. (4) and (5)]. Note that this criterion was arbitrary and represents a good compromise between the experimental and numerical uncertainties and the need to obtain a reasonable yet conservative criteria for the transition between the two regimes.

Tien and Drolen [15] reviewed experimental studies considering the scattering efficiency factor, scattering cross-section, or scattering coefficient of suspensions of latex particles in water or air [27,36–40] and of various pigment suspensions in water [41] with $0.05 \leq \chi_s \leq 400$ and $10^{-6} \leq f_v \leq 0.74$. The review also included two analytical studies [30,42]. The different experimental studies established the transition between the independent and dependent scattering regimes corresponding to $\bar{c}/r_s$ ranging between 0.8 and 1.4 and $\bar{c}^*$ around 0.3-0.5 depending of the suspensions considered. The authors also presented a scattering regime map in the diagram plotting the particle size parameter χ_s versus particle volume fraction f_v based on the work of Yamada et al. [40] for monodisperse latex particles in water or air (m = 1.2 or 1.6) with $0.2 \leq \chi_s \leq 90$ and $10^{-3} \leq f_v \leq 0.74$. For $\chi_s \leq 0.388$, the critical particle volume fraction corresponding to the independent/dependent scattering transition was $f_{v,\,cr} = 0.006$ [15]. On the other hand, for $\chi_s > 0.388$ and $f_v > 0.006$, the transition from independent to dependent scattering was given by a critical average clearance-to-wavelength ratio of [15]

$$\bar{c}^*_{cr} = 0.5. \tag{6}$$

The corresponding critical particle volume fraction $f_{v,\,cr}$ was calculated by assuming a rhombohedral packing of monodisperse particles and expressed as [15]

$$f_{v,cr} = \left(\frac{0.9047}{\pi/2\chi_s + 1}\right)^3. \tag{7}$$

Kaviany and Singh [17] modified the average clearance distance $\bar{c}$ proposed by Tien and Drolen [15] by $\bar{c}$+0.2r_s where the distance 0.2r_s was added in an ad hoc manner to correct for the close-pack separation distance in a rhombohedral packing when the most compact arrangement is obtained (i.e., $f_v = 0.74$) to yield [17]

$$\bar{c}^*_{cr} = 0.5 - 0.1\chi_s/\pi \quad \text{resulting in} \quad f_{v,cr} = \left(\frac{0.9047}{\pi/2\chi_s + 0.9}\right)^3. \tag{8}$$

This correction was negligible for systems with particle volume fraction $f_v < 0.3$ but resulted in a significant difference between Eqs. (7) and (8) for particle volume fraction $f_v > 0.5$ [17]. Eq. (8) was shown to predict experimental data for monodisperse latex spheres in water and air [40] more closely than Eqs. (6) and (7). Although these studies [15,17] considered experimental data covering a wide range of particle size parameters $0.2 \leq \chi_s \leq 90$, they considered non-absorbing monodisperse particles with relative index of refraction m of either 1.2 (latex particles in water) or 1.6 (latex particles in air). Note that Tien and Drolen [15] did not consider the scattering phase function or asymmetry factor of the suspensions.

Olaofe [19] derived an analytical expression for the scattering cross-section of bispheres by integrating the scattered field intensity obtained from solving Maxwell's equations. In particular, the author presented the ratio of some scattering efficiency factors of non-absorbing monodisperse bispheres defined as $Q^b_{sca} = C^b_{sca}/\pi r_s^2$ to that of a single sphere Q^M_{sca} predicted by Lorenz-Mie theory. Here, C^b_{sca} was the scattering cross-section of the bisphere at a fixed orientation, the particle size parameter χ_s was 0.5 or 1, and m ranged from 1.05 to 1.50. The ratio Q^b_{sca}/Q^M_{sca} was plotted as a function of the ratio d^* between $1/2\pi$ and $15/\pi$. As the separation distance between the spheres increased, the oscillation amplitude decreased and Q^b_{sca}/Q^M_{sca} tended asymptotically towards 2 corresponding to the independent scattering regime when $Q^b_{sca} = 2Q^M_{sca}$ [19]. Moreover, the oscillation pattern of the ratio Q^b_{sca}/Q^M_{sca} was shown to vary with changes in the bisphere orientation. Finally, Olaofe [19] concluded that the relative index of refraction m

$= n_s/n_m$ did not affect the efficiency factor ratio Q^b_{sca}/Q^M_{sca} when all other parameters were kept constant.

Videen et al. [28] developed a general expression for the orientation-averaged asymmetry factor of monodisperse bispheres using an extension of Lorenz-Mie theory. The expression consisted of one term accounting for far-field interferences and another accounting for near-field interactions. The bispheres consisted of two absorbing monodisperse carbon spheres with $\chi_s = 0.628$ or 3.14 and $m = 1.75 + i0.44$. The authors showed that far-field interferences resulted in enhanced forward scattering due to constructive interference in the forward direction. On the other hand, near-field interactions resulted in enhanced backscattering "due to constructive interference of rays reflecting off multiple interfaces" [28]. Lastly, they showed that the asymmetry factor of bispheres tended towards the asymmetry factor of a single sphere when the interparticle distance-to-wavelength ratio d^* exceeded 2.

Quirantes et al. [16] used the T-matrix algorithm to predict the orientation-averaged scattering cross-section ratio $C^b_{sca}/2C^M_{sca}$ of non-absorbing monodisperse bispheres with particle size parameter χ_s varying from 0.1 to 20, interparticle distance-to-radius ratio d/r_s varying from 2 to 20, and relative index of refraction $m = 1.2$. The critical interparticle distance-to-radius ratio $(d/r_s)_{cr}$ was estimated for bispheres with different particle size parameter χ_s. The authors also hypothesized that the critical criterion obtained for bispheres could be extended to particle suspensions. Then, the critical particle volume fraction $f_{v,\,cr}$ beyond which dependent scattering prevailed was such that [16]

$$f_{v,cr} = \frac{4}{3}\pi\left(\frac{r_s}{d}\right)^3. \tag{9}$$

The authors showed that when $\chi_s < 5.5$ the critical particle volume fraction $f_{v,\,cr}$ decreased with decreasing χ_s. In particular, suspensions of monodisperse particles such that $\chi_s < 1$ fell in the independent scattering regime for $f_{v,\,cr} < 0.001$. Note that this criterion contradicts that proposed by Tien and Drolen [15] and such that $f_{v,\,cr} = 0.006$ for suspensions of particles with $\chi_s < 0.388$.

Mishchenko et al. [6] studied the orientation-averaged phase function and scattering matrix elements of monodisperse bispheres with $\chi_s = 5$ and 15 and $m = 1.5 + i0.005$ using the T-matrix algorithm. The authors showed that, in both cases, the independent scattering regime was reached when the interparticle distance d exceeded four times the particle radius r_s, i.e., $d/r_s \geq 4$. In addition, Mishchenko et al. [18] studied the independent and dependent scattering regimes of 8 non-absorbing monodisperse spheres randomly distributed but in contact with at least another sphere. The particle size parameter was $\chi_s = 4$, the relative index of refraction m was 1.32, and the particle volume fraction f_v varied from 0.0014 to 0.296. The authors showed that the scattering cross-section ratio $C^s_{sca}/8C^M_{sca}$ and forward-scattering phase function ratio $\Phi^s(\Theta = 0)/8\Phi^M(\Theta = 0)$ tended towards 1 when the average interparticle distance-to-wavelength ratio was such that $2\pi\bar{d}^* > 30$ and $f_v < 0.01$. Here, $\Phi^s(\Theta = 0)$ and $\Phi^M(\Theta = 0)$ are the phase functions of the particle suspension and of a single particle in the forward direction ($\Theta = 0^\circ$), respectively. Furthermore, the study showed that near-field interactions resulted in enhanced backscattering, in agreement with Videen et al. [28]. Especially, multiple scattering was shown to corroborate with "the interference nature of coherent backscattering".

Ivezić and Mengüç [20] used the discrete dipole approximation (DDA) method to study a system of two monodisperse carbon spheres with $m = 1.75 + i0.75$ and $0.2 \leq \chi_s \leq 1$ under polarized incident radiation. Their study focused on the scattering cross-section and phase function of bispheres at fixed orientations and established that the independent scattering regime was reached for a critical clearance-to-radius ratio given by [20]

$$(c/r_s)_{cr} = 2/\chi_s. \tag{10}$$

The authors also studied touching aligned spheres and ordered aggregates (e.g., tetrahedron, body centered cubes, etc.) with up to 12 monodisperse spheres. Orientation-averaged results for agglomerates showed that when $\chi_s \approx 2$, the scattering cross-section and phase function were within 10–20% of the independent scattering regime predictions. Then, they concluded that "dependent effects never disappear" for such systems due to the adjacency of the particles.

Ivezić et al. [34] also studied the effect of the relative index of refraction m on the parameter $(C^s_{sca}/C^M_{sca})(C^M_{abs}/C^s_{abs})(\Phi^s/\Phi^M)$ of aggregates on the basis that dependent effects on C^s_{sca}, C^s_{abs}, and Φ^s "are difficult to separate" [34]. Here, C^s_{abs} is the absorption cross-section of the particle system. Results for compact and linear aggregates with 7 monodisperse spheres with a particle size parameter χ_s varying from 0.025 to 1.57 and for the scattering angles $\Theta = 45$, 135, and 165° were presented. First, the particle index of refraction n_s was taken as $n_s = 1.75$ while the absorption index was $k_s = 0.01$, 0.1, or 1. Second, the absorption index was kept constant as $k_s = 0.75$ and the index of refraction n_s was taken as equal to 1.5, 1.75, or 2.0. The authors concluded that the complex index of refraction had a negligible effect on the parameter $(C^s_{sca}/C^M_{sca})(C^M_{abs}/C^s_{abs})(\Phi^s/\Phi^M)$. The study's conclusion suggests that the complex index of refraction m did not affect the transition between the scattering regimes for particle suspensions.

Ma et al. [35] investigated densely packed disordered aggregates with $N_s = 200$ monodisperse particles with size parameter $\chi_s = 6.964$ (corresponding to $r_s = 500$ nm and $\lambda = 600$ nm) embedded in a virtual spherical domain of radius equal to $10r_s$ in water (i.e., $n_m = 1.33$). The index of refraction of the particles n_s varied from 1.4 to 3.0 and the absorption index k_s from 0 to 1.0. The Mueller matrix elements of the scattering system were computed using the T-matrix method. The authors concluded that the transition between independent and dependent scattering regimes depended not only on the clearance-to-wavelength ratio c^* but also on the complex index of refraction m. However, this conclusion was in contradiction with those of Olaofe [19] and Ivezić et al. [34]. This disagreement could be due to the fact that different particle systems with different particle size parameter χ_s and relative index of refraction m were considered.

Table 1 summarizes the range of parameters explored in the different studies previously reviewed and the transition criteria proposed. First, most studies considered a narrow range of particle size parameter χ_s and/or relative complex index of refraction m. Second, major discrepancies appear in the choice of parameters governing the scattering cross-section and asymmetry factor as well as the transition criteria between independent and dependent scattering regimes.

The present study aims to investigate scattering by non-absorbing bispheres, particle suspensions, as well as aggregates with a wide range of particle size parameter ($0.031 \leq \chi_s \leq 8.05$) and relative index of refraction ($0.677 \leq m \leq 2.6$). This study focuses on integral radiative characteristics, namely the scattering cross-section and asymmetry factor, because they are essential in solving the RTE in applications concerned with unpolarized light such as those illustrated in Fig. 1. The goal of this study is (i) to determine unequivocally the parameters controlling the scattering cross-section and asymmetry factor of bispheres, suspensions, and aggregates of non-absorbing monodisperse spherical particles, (ii) to assess the validity of the transition criteria between the independent and dependent scattering regimes proposed in the literature (Table 1) and, if necessary, propose an alternative criterion, and (iii) to determine whether transition criteria for bispheres can be extrapolated to particle suspensions and aggregates, as previously assumed in the literature [16].

3. Analysis

3.1. Computer-generated structures

The radiative characteristics of three types of non-absorbing particle arrangements were investigated namely (i) bispheres, (ii) multiple disordered, monodisperse, non-touching spherical particles representative of particle suspensions, and (iii) multiple ordered monodisperse touching or non-touching spherical particles. Radiative characteristics of bispheres were denoted by the superscript "b" and those of disordered and ordered particle systems were denoted by the superscript "s". Figs. 2(a)-2(c) illustrate the investigated bispheres and the disordered particle systems obtained by randomly generating 4 or 8 particles in a cubic domain of size L and volume $V_{tot} = L^3$. Figs. 2(d)–2(g) display ordered particle systems including tetrahedron and simple cubic structures with $N_s = 4$ or 8 when the particles were touching [Figs. 2(b) and 2(c)] and non-touching [Figs. 2(d) and 2(e)]. For any given arrangement, all spherical particles had a radius r_s ranging from 2.5 nm to 50 nm while wavelength λ was varied so that the particle size parameter χ_s ranged from 0.031 to 8.05. In addition, the non-absorbing particle relative index of refraction m varied from 0.667 to 2.6. To investigate both dependent and independent scattering regimes, the size of the cubic domain or lattice was progressively increased resulting in increasing interparticle distances d. For bispheres, the interparticle distance d ranged from 5 nm to 30 μm. In the case of disordered and ordered particle systems, the average interparticle distance $\bar{d}$ ranged from 25 nm to 1.4 μm.

3.2. Scattering characteristics

The discrete-dipole approximation (DDA) algorithm developed by Draine and Flatau [31] was used to compute the scattering cross-section C_{sca} and asymmetry factor g of the different particle systems considered. First, N_d cubic dipoles of side Δd were generated inside the N_s particles. The dipoles were such that their size Δd was small compared to the particle radius r_s and wavelength λ to achieve numerically converged results independent of the choice of discretization [43]. The input parameters of the DDA method included (i) the position of the N_d cubic dipoles, (ii) the wavelength λ, (iii) the particle relative index of refraction m with respect to the surrounding, and (iv) the equivalent radius r_{eq} defined as the radius of a sphere with the same volume V_s as the particle system and expressed as [43]

$$r_{eq} = \left(\frac{3V_s}{4\pi}\right)^{1/3}. \tag{11}$$

Substituting Eq. (3) into Eq. (11) simplifies the equivalent radius as $r_{eq} = {N_s}^{1/3} r_s$. The scattering cross-section C_{sca} (in nm^2) of systems consisting of N_s monodisperse particles was expressed as a function of the computed scattering efficiency factor Q_{sca} according to [43]

$$C_{sca} = \pi r_{eq}^2 Q_{sca}. \tag{12}$$

The scattering cross-section C_{sca} and asymmetry factor g were averaged over at least 33 orientations for bispheres and simple cubic structures and over at least 115 orientations for tetrahedrons and disordered particle systems to ensure accurate orientation-averaging. Similarly, the number of scattering directions was set greater than 1000 so that the asymmetry factor g can be properly estimated [Eq. (2)]. Finally, the DDA method was validated against predictions by Lorenz-Mie theory for single spheres with particle size parameter χ_s and relative index of refraction m in the same range as that of the particle systems investigated. In all cases, predictions of C_{sca} and g by the DDA method fell within 3% of those by Lorenz-Mie theory (see Figs. S1 and S2 in Supporting Information). In fact, the average error between the two methods was 0.89% for the scattering cross-section and 0.85% for the asymmetry factor for all cases considered in the validation.

4. Results and discussion

4.1. Bispheres

4.1.1. Governing dimensionless parameters

Fig. 3 plots (left) the scattering cross-section C_{sca}^b of bispheres as a function of the interparticle distance d and (right) the scattering cross-section ratio $C_{sca}^b/2C_{sca}^M$ as a function of the interparticle distance-to-wavelength ratio $d^* = d/\lambda$ for bispheres with $m = 1.5$ and (a) $\chi_s = 0.031$, (b) $\chi_s = 0.063$, and (c) $\chi_s = 0.126$. Each size parameter χ_s was represented by three cases corresponding to different values of particle radius r_s and wavelength λ. Fig. 3 indicates that the scattering cross-section C_{sca}^b plotted as a function of d differed significantly among cases with the same particle size parameter χ_s but different particle radius r_s and wavelength λ. By contrast, the scattering cross-section ratio $C_{sca}^b/2C_{sca}^M$ plotted as a function of the interparticle distance-to-wavelength ratio d^* collapsed on a single line for any given particle size parameter χ_s. Similar results were obtained for different values of m including 1.2 and 2 (see Fig. S3 in Supporting Information). These results establish that the ratio $C_{sca}^b/2C_{sca}^M$ was a function of only χ_s, m, and d^*, i.e., $C_{sca}^b(\chi_s, m, d^*, r_s) = 2f^b(\chi_s, m, d^*)C_{sca}^M(\chi_s, m, r_s)$ where f^b is a function to be determined. Note that the parameters c^*, c/r_s, and d/r_s can be expressed in terms of both the interparticle distance-to-wavelength ratio d^* and particle size parameter χ_s such that

$$c^* = d^* - \chi_s/\pi, \quad c/r_s = \frac{2\pi}{\chi_s} d^* - 2, \quad \text{and} \quad d/r_s = \frac{2\pi d^*}{\chi_s}. \tag{13}$$

Therefore, $C_{sca}^b(\chi_s, m, d^*, r_s)$ could also be expressed in terms of c^*, c/r_s, or d/r_s instead of d^*. However, plotting $C_{sca}^b/2C_{sca}^M$ versus c^*, c/r_s, or d/r_s for the three particle size parameter $\chi_s = 0.031$, 0.063, and 0.126 did not result in the collapse of the data on a single line such as that observed when plotting versus d^* (Fig. S4 in Supporting Information). Therefore, χ_s, m, and d^* are the independent parameters determining the scattering cross-section ratio $C_{sca}^b/2C_{sca}^M$ of bispheres.

Moreover, Fig. 3 shows that when the two spheres were touching (i.e., $d = 2r_s$ and $d^* = \chi_s/\pi$) the bisphere scattering cross-section was 4 times that of a single sphere, i.e., $C_{sca}^b = 4C_{sca}^M$, for the values of χ_s considered. Similar observations were also reported in Refs. [6,16]. This observation can be explained by the so-called equivalent volume model consisting of approximating the scattering cross-section of a particle aggregate as that of an equivalent sphere with the same volume V_s and an equivalent radius $r_{eq} = {N_s}^{1/3} r_s$ [14]. In fact, since the scattering cross-section of particles in the Rayleigh regime is proportional to the square of the volume V_s [Eq. (1)], expressing the scattering cross-section C_{sca}^R of an aggregate using Eq. (1) with $V_s = (4\pi/3)r_{eq}^3$ results in

$$C_{sca}^R = N_s^2 C_{sca}^M. \tag{14}$$

In other words, for touching bispheres $C_{sca}^{b,R} = 4C_{sca}^M$. This also indicates that the equivalent volume model was valid for aggregates with touching particles for the size parameter χ_s considered. This was in agreement with previous studies investigating the validity of the equivalent volume model for aggregates with small particles [14].

Fig. 3 also demonstrates that when the interparticle distance-to-wavelength ratio d^* exceeded 2, independent scattering prevailed since $C_{sca}^b \simeq 2C_{sca}^M$. On the other hand, when $d^* < 2$, the ratio $C_{sca}^b/2C_{sca}^M$ oscillated and exceeded 1 for the values of χ_s and m considered. This was due to dependent effects and notably

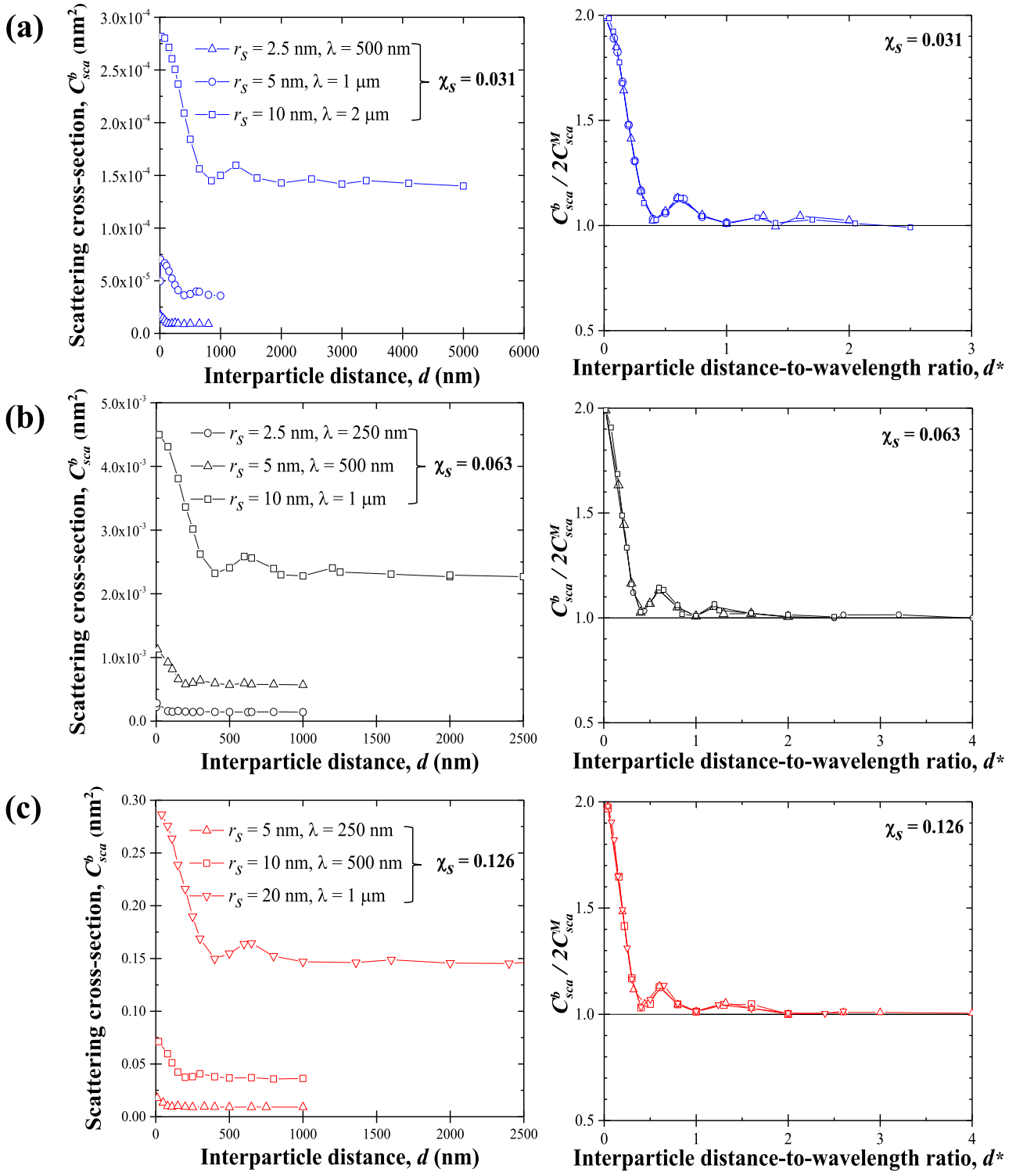

Fig. 3. (left) Scattering cross-section C^b_{sca} as a function of the interparticle distance d and (right) corresponding scattering cross-section ratio $C^b_{sca}/2C^M_{sca}$ as a function of the interparticle distance-to-wavelength ratio d^* of bispheres for (a) $\chi_s = 0.031$, (b) $\chi_s = 0.063$, and (c) $\chi_s = 0.126$ and $m = 1.5$.

to interference effects. These results were in agreement with published numerical simulations for bispheres with small size parameter [6,16].

Fig. 4 shows (left) the asymmetry factor g^b as a function of the interparticle distance d and (right) the asymmetry factor g^b as a function of the interparticle distance-to-wavelength ratio d^* for bispheres with $m = 1.5$ and (a) $\chi_s = 0.031$, (b) $\chi_s = 0.063$, and (c) $\chi_s = 0.126$. The different cases corresponded to those shown in Fig. 3 for C^b_{sca}. Fig. 4 indicates that the asymmetry factor g^b of bispheres with the same particle size parameter χ_s but different radius r_s and wavelength λ differed when plotted as a function of d. However, the different plots of g^b for a given value of χ_s overlapped when plotted as functions of d^*. In other words, the asymmetry factor g^b could also be expressed as a function of χ_s, m, and

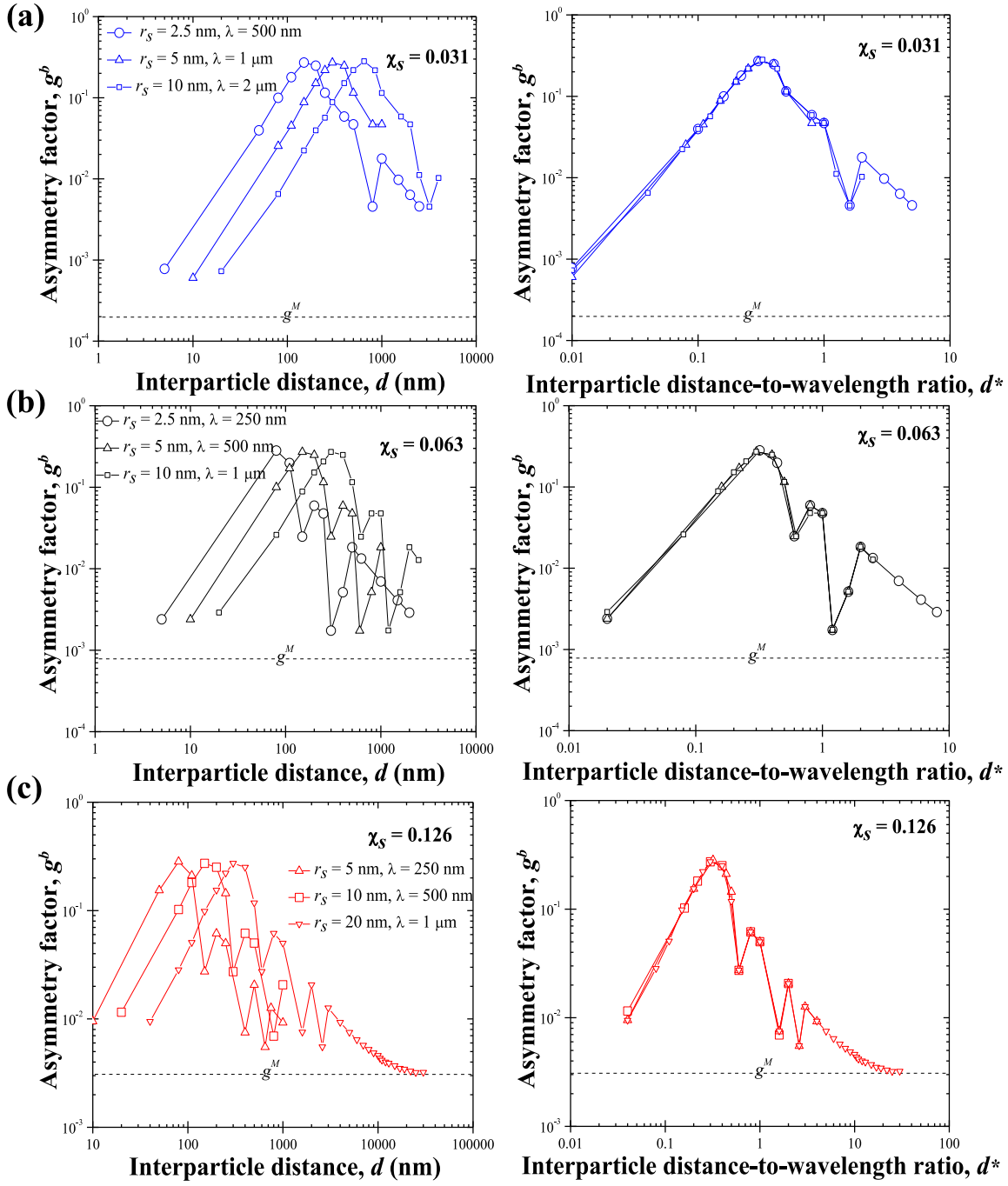

Fig. 4. (left) Asymmetry factor g^b of bispheres as a function of the interparticle distance d and (right) asymmetry factor g^b as a function of the interparticle distance-to-wavelength ratio d^* of bispheres for (a) $\chi_s = 0.031$, (b) $\chi_s = 0.063$, and (c) $\chi_s = 0.126$ and $m = 1.5$.

d^*, i.e., $g^b = g^b(\chi_s, m, d^*)$, as previously established for $C^b_{sca}/2C^M_{sca}$. The same conclusions were reached for $m = 1.2$ and 2 (Fig. S5 in Supporting Information). Moreover, the parameters χ_s, m, and d^* were also shown to be the independent parameters controlling the asymmetry factor of bispheres (Fig. S6 in Supporting Information). Finally, it is interesting to note that the bisphere asymmetry factor g^b converged towards that of a single sphere g^M but for $d^* \geq 25$ instead of $d^* \geq 2$ as observed for C^b_{sca} (Fig. 3).

4.1.2. Bisphere scattering cross-section C^b_{sca}

Fig. 5 presents the scattering cross-section ratio $C^b_{sca}/2C^M_{sca}$ as a function of the interparticle distance-to-wavelength ratio d^* of bispheres with $m = 1.5$ and (a) $\chi_s \leq 2$ and (b) $\chi_s > 2$. Fig. 5(a) indicates that for $\chi_s \leq 2$ and $d^* < 2$, dependent effects due to interactions and interferences between the two particles resulted in the scattering cross-section of the bisphere exceeding that of two individual spheres, i.e., $C^b_{sca} > 2C^M_{sca}$, as previously observed in Fig. 3. Furthermore, the oscillations in $C^b_{sca}/2C^M_{sca}$, observed for $\chi_s \leq 2$ and $d^* < 2$, reached their maxima and minima for the same values of d^* for all particle size parameter χ_s considered. This suggests that the interparticle distance-to-wavelength ratio d^* determined if interferences between waves scattered by each sphere were constructive or destructive. This also further confirms that χ_s, m, and d^* are the independent parameters determining the effect of dependent scattering on the scattering cross-section of bispheres. Interestingly, the subsequent maxima and minima were

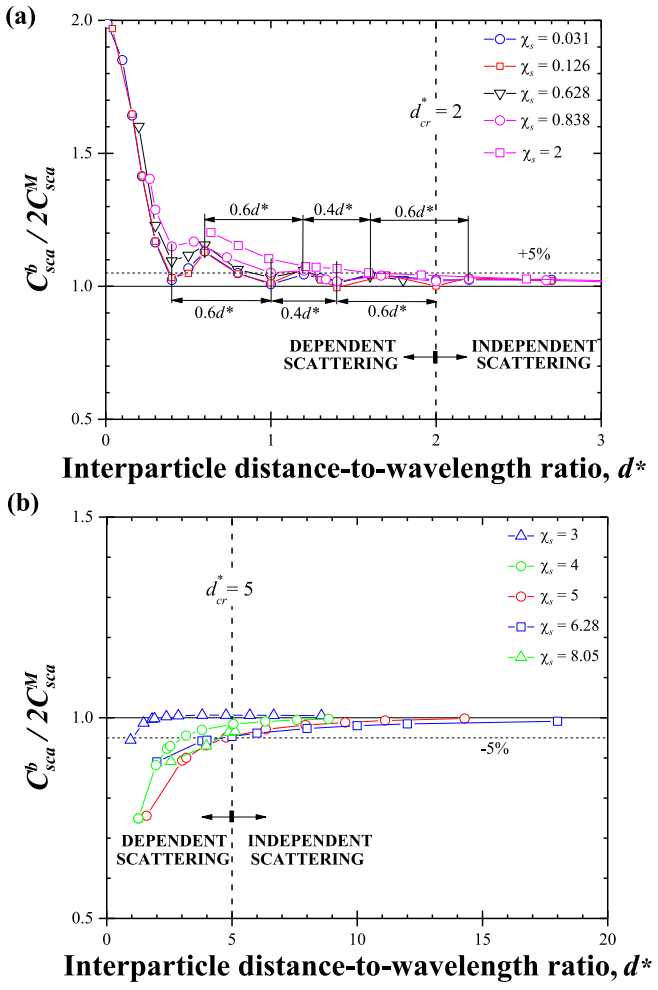

Fig. 5. Scattering cross-section ratio $C^b_{sca}/2C^M_{sca}$ as a function of the interparticle distance-to-wavelength ratio d^* for bispheres with $m = 1.5$ and (a) $\chi_s \leq 2$ and (b) $\chi_s > 2$.

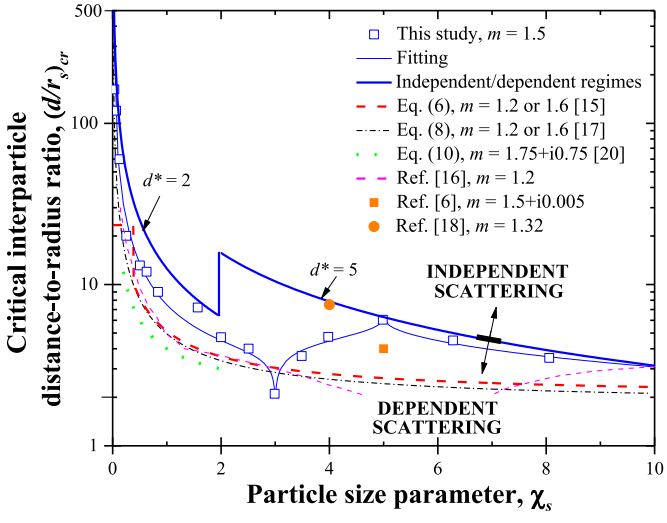

Fig. 6. Critical interparticle distance-to-radius ratio $(d/r_s)_{cr}$ as a function of particle size parameter χ_s for bispheres with $m = 1.5$ along with data and predictions from expressions reported in the literature [6,15–18,20] and summarized in Table 1. The data points collected for the present study were fitted to a power series to guide the eye.

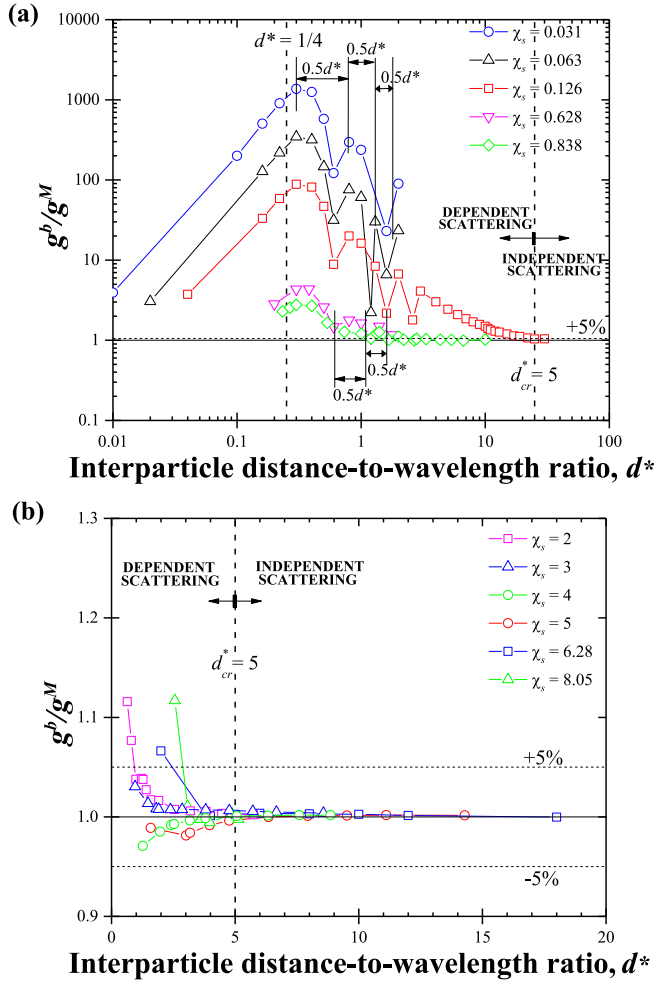

Fig. 7. Asymmetry factor ratio g^b/g^M as a function of the interparticle distance-to-wavelength ratio d^* for bispheres with $m = 1.5$ and (a) $\chi_s \leq 2$ and (b) $\chi_s > 2$.

spaced by the same interparticle distance-to-wavelength ratio d^* of approximately 1/2. This observation was also made by Videen et al. [28] regarding the subsequent maxima of the interference term of the asymmetry factor. By contrast, Fig. 5(b) shows that for large bispheres with $\chi_s > 2$, the scattering cross-section ratio $C^b_{sca}/2C^M_{sca}$ did not feature any oscillation. Moreover, dependent effects caused the scattering cross-section C^b_{sca} of the bisphere to be smaller than the scattering cross-section of two individual spheres, i.e., $C^b_{sca} < 2C^M_{sca}$. These observations were also consistent with those made in previous studies [6,16].

Finally, Fig. 5 establishes that the independent scattering regime for bispheres prevailed, i.e., $C^b_{sca} = 2C^M_{sca}$ when d^* exceeded a critical value d^*_{cr} such that (a) $d^*_{cr} = 2$ for $\chi_s \leq 2$ and $m = 1.5$ and (b) $d^*_{cr} = 5$ for $2 < \chi_s \leq 8.05$ and $m = 1.5$.

4.1.3. Critical interparticle distance-to-radius ratio $(d/r_s)_{cr}$

In some studies, the ratio d/r_s was preferred over $d^* = d/\lambda$ to identify the transition between dependent and independent scattering regimes [6,16]. As indicated in Eq. (13), the critical interparticle distance-to-radius ratio $(d/r_s)_{cr}$ can be expressed as a function of the critical interparticle distance-to-wavelength ratio d^*_{cr}. In order to facilitate the comparison of the different studies summarized in Table 1, Fig. 6 displays the critical interparticle distance-to-radius ratio $(d/r_s)_{cr}$ for bispheres or suspensions as a function of particle size parameter χ_s reported in previous studies [6,15–18,20] for different particle relative index of refraction m. Note that

Table 1
Literature review of studies on independent and dependent scattering regimes.

Reference	[6]	[15]	[16]	[17]	[18]	[20]
Type of study	Simulations	Review	Simulations	Review	Simulations	Simulations
Data from	T-matrix	Experiments	T-matrix	Experiments	T-matrix	DDA
Particle system	Bisphere	Suspension and aggregate	Bisphere	Suspension and aggregate	Suspension	Bisphere and aggregate
Radiation characteristics	Scattering matrix elements, Q_{sca}	Q_{sca}	C_{sca}	Q_{sca}	C_{sca}, Φ	C_{sca}, Φ
Relative index of refraction m	1.5+i0.005	1.2 and 1.6	1.2	1.2 and 1.6	1.32	1.75+i0.75
Particle size parameter χ_s	$\chi_s = 5$ and 15	$0.2 \le \chi_s \le 90$	$0.1 \le \chi_s \le 20$	$0.2 \le \chi_s \le 90$	$\chi_s = 4$	$0.2 \le \chi_s \le 2$
Particle volume fraction f_v	N/A	$10^{-3} \le f_v \le 0.74$	N/A	$10^{-3} \le f_v \le 0.74$	$0.0014 \le f_v \le 0.30$	N/A
Critical criteria[1]	$(d/r_s)_{cr} \simeq 4$	$\bar{c}^*_{cr} = 0.5$ ($\chi_s > 0.388$)	$(d/r_s)_{cr}$ plotted	$\bar{c}^*_{cr} = 0.5 - 0.1\chi_s/\pi$	$\bar{d}^*_{cr} \ge 15/\pi$	$(c/r_s)_{cr} = 2/\chi_s$
$f_{v,cr}$ =[1]	N/A	0.006 ($\chi_s < 0.388$) $(\frac{0.9047}{\pi/2\chi_s+1})^3$ ($\chi_s > 0.388$)	$\frac{4\pi}{3}(\frac{1}{(c/r_s)_{cr}+2})^3$	$(\frac{0.9047}{\pi/2\chi_s+0.9})^3$	$f_{v,cr} < 0.01$	N/A

[1] The independent scattering regime prevailed for values of d^*, c^*, c/r_s, and d/r_s above the critical criteria and values of f_v below $f_{v,cr}$.

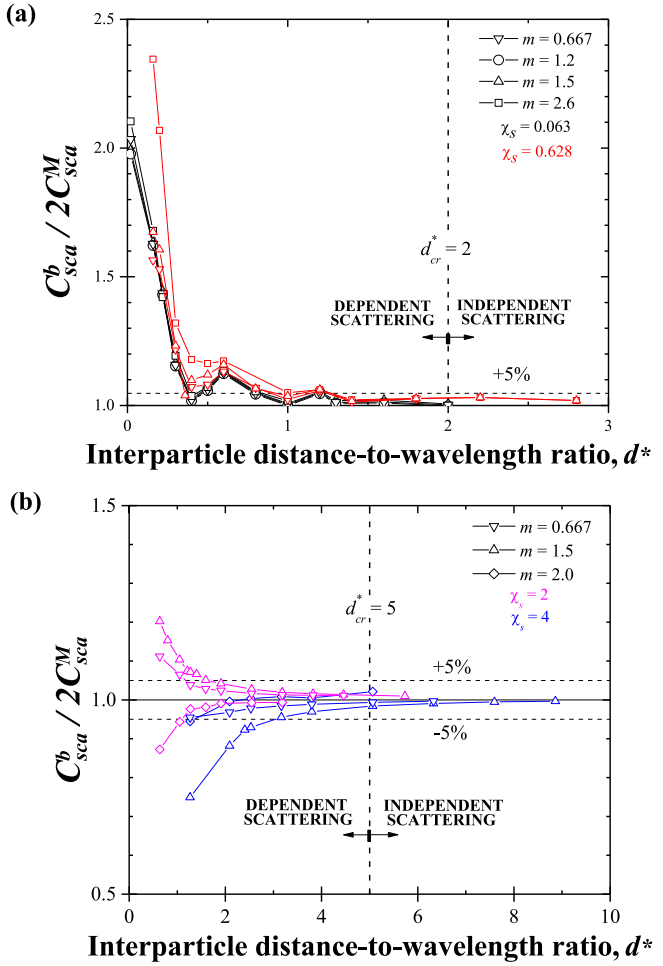

Fig. 8. Scattering cross-section ratio $C^b_{sca}/2C^M_{sca}$ as a function of the interparticle distance-to-wavelength ratio d^* for bispheres with m varying between 0.667 and 2.6 and (a) $\chi_s = 0.063$ and 0.628 and (b) $\chi_s = 2$ and 4.

when particle suspensions were investigated, the parameter considered was in fact the critical average interparticle distance-to-radius ratio $(\bar{d}/r_s)_{cr}$ [15,17,18]. In the present study, $m = 1.5$ and d^*_{cr}, used in the calculation of $(d/r_s)_{cr}$, was determined from data shown in Fig. 5 when the scattering cross-section of bispheres fell within 5% of predictions by Lorenz-Mie theory, i.e., when $|1 - C^b_{sca}/2C^M_{sca}| \le 0.05$. First, Fig. 6 indicates that the different models [15,17,20] and numerical results [6,16,18] predicting the transition between the dependent and independent scattering regimes differed significantly from one another and from results obtained in the present study. However, Fig. 6 indicates that the numerical predictions for $(d/r_s)_{cr}$ reported in Ref. [16] for $m = 1.2$ were in qualitative agreement with those of the present study for $m = 1.5$.

Finally, Fig. 6 indicates that the transition criteria $d^*_{cr} = 2$ for $\chi_s \le 2$ and $d^*_{cr} = 5$ for $\chi_s > 2$ from dependent to independent scattering regimes encompass all the criteria previously reported. In practice, the critical interparticle distance d_{cr} to ensure the independent scattering regime was such that $d_{cr} \ge 6.5r_s$ for $\chi_s \ge 2$. However, for $\chi_s < 0.2$, independent scattering prevailed for interparticle distance d hundreds of time larger than the particle radius r_s, i.e., $d_{cr} \ge 100r_s$.

4.1.4. Bisphere asymmetry factor g^b

Fig. 7 plots the ratio g^b/g^M of the asymmetry factor g^b for bispheres to that predicted by Lorenz-Mie theory g^M for a single particle as a function of the interparticle distance-to-wavelength ratio d^* for spheres with $m = 1.5$ and (a) $\chi_s < 2$ and (b) $\chi_s \ge 2$. First, Fig. 7 indicates that for particle size parameter $\chi_s \le 2$, the asymmetry factor ratio g^b/g^M vs. d^* featured oscillations whose magnitude tended to decrease with increasing χ_s. In fact, these oscillations disappeared for $\chi_s \ge 2$ [Fig. 7(b)], as also observed in $C^b_{sca}/2C^M_{sca}$ vs. d^* [Fig. 5(b)]. Furthermore, for $\chi_s < 2$ the oscillations reached their maxima and minima for the same values of d^* as observed for $C^b_{sca}/2C^M_{sca}$ [Fig. 5(a)]. Moreover, g^b/g^M reached a global maximum around $d^* = 1/4$ and the subsequent maxima and minima occured at intervals of approximately 1/2, in agreement with observations made by Videen et al. [28]. The global maximum was attributed to destructive interferences of the scattered radiation by individual particles.

Finally, Fig. 7 indicates that g^b/g^M converged towards unity (i.e., $g^b = g^M$) as d^* increased beyond a critical interparticle distance-to-wavelength ratio d^*_{cr} when independent scattering regime prevailed. For small particles such that $\chi_s < 2$, the smaller the particles, the larger the critical interparticle distance-to-wavelength ratio d^*_{cr}. For example, the critical interparticle distance-to-wavelength ratio d^*_{cr} was 2 for $\chi_s \ge 0.628$ but reached 25 for $\chi_s = 0.126$. On the other hand, for large particles such that $\chi_s \ge 2$, independent scattering for g^b prevailed for $d^* \ge 5$, as obtained also for C^b_{sca}.

Overall, this study showed that the particle size parameter χ_s and interparticle distance-to-wavelength ratio d^* are the dimensionless parameters governing the scattering cross-section and asymmetry factor of bispheres. The fact that χ_s is one parameter controlling scattering of light is well-known for single-particles

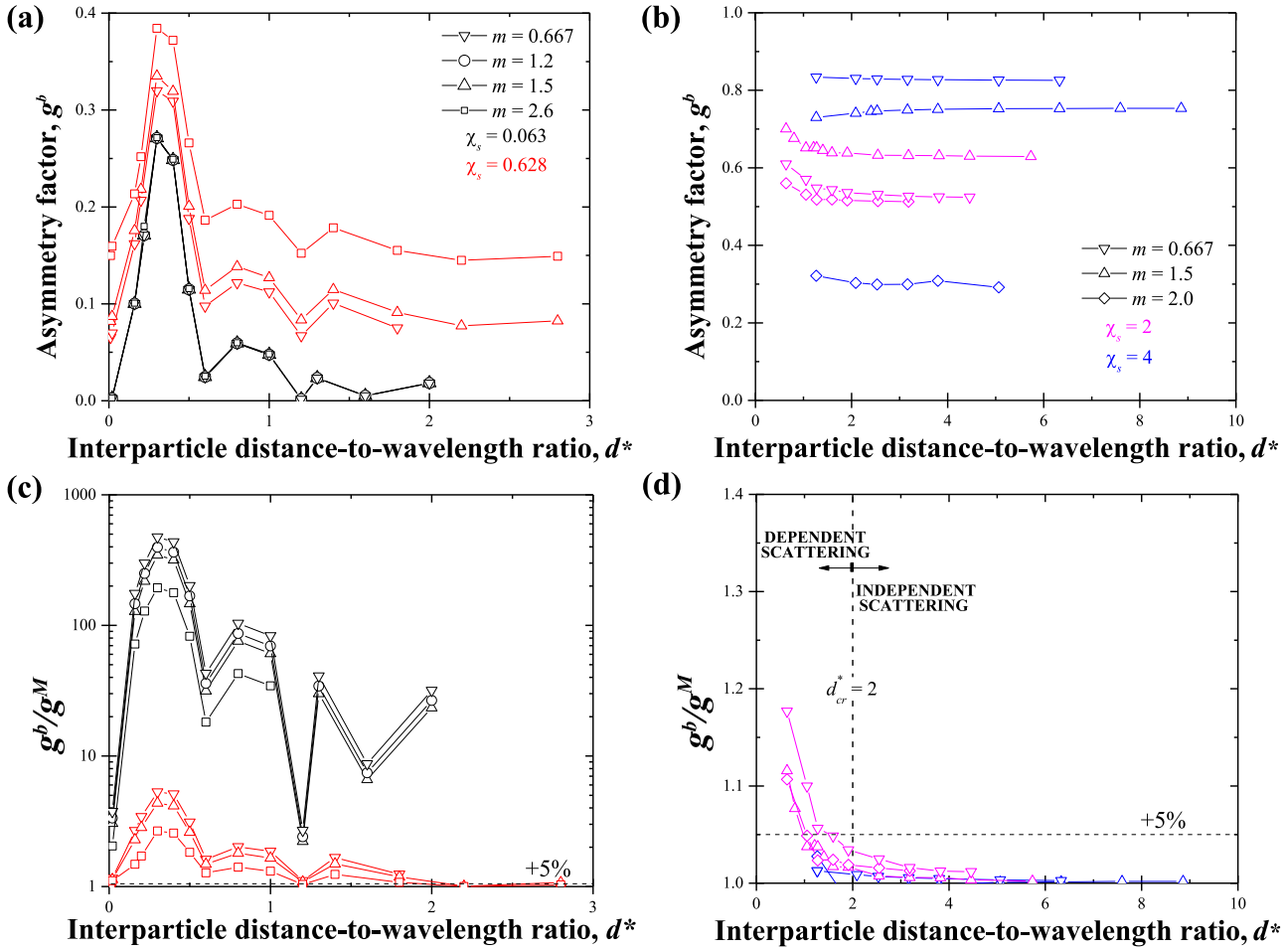

Fig. 9. Asymmetry factor g^b as a function of the interparticle distance-to-wavelength ratio d^* for bispheres with m varying between 0.667 and 2.6 and (a) $\chi_s = 0.063$ and 0.628 and (b) $\chi_s = 2$ and 4.

[21]. However, to the best of our knowledge, this has not been demonstrated for particle systems. Similarly, the present study establishes unequivocally that d^* is the dimensionless distance parameter controlling interference effects. Note that all the results discussed so far for C^b_{sca} and g^b of bispheres were obtained for the same value of relative particle index of refraction $m = n_s/n_m = 1.5$. Thus, it is essential to consider different values of m to fully assess the validity of the above conclusions.

4.2. Effect of the relative index of refraction m

4.2.1. Effect of m on the scattering cross-section C^b_{sca}

Fig. 8 plots the scattering cross-section ratio $C^b_{sca}/2C^M_{sca}$ as a function of the interparticle distance-to-wavelength ratio d^* for bispheres with particle size parameter (a) $\chi_s = 0.063$ or 0.628 and (b) $\chi_s = 2$ or 4 and relative index of refraction m varying between 0.667 and 2.6. It indicates that the scattering cross-section ratio $C^b_{sca}/2C^M_{sca}$ of bispheres was independent of the relative index of refraction m for very small particle size parameter such as $\chi_s = 0.063$ as well as for $\chi_s = 0.628$ with small index mismatch ($m \leq 1.2$). This could be attributed to the fact that for small size parameter χ_s (i) the phase shift $\beta = 2\chi_s|m-1|$ was negligible and (ii) scattering was isotropic ($g^M \simeq 0$). Then, interference and interaction effects were independent of m. These results establish that C^b_{sca} can be expressed as $C^b_{sca} = 2f^b(d^*)C^M_{sca}(\chi_s, m, r_s)$ for $\chi_s|m-1| \ll 1$ where $f^b(d^*)$ is a function to be determined.

By contrast, the scattering cross-section ratio $C^b_{sca}/2C^M_{sca}$ of bispheres with $\chi_s = 2$ and 4 as well as $\chi_s = 0.628$ and $m \geq 1.5$ depended on the relative index of refraction m. Here, the phase shift across the particles was significant (e.g., $\beta = 2$ for $\chi_s = 0.628$ and $m = 2.6$) and interference effects were affected by changes in m. Moreover, scattering of the particles was anisotropic and more sensitive to m.

Finally, Fig. 8 establishes that, here also, and regardless of m, the independent scattering regime, characterized by $C^b_{sca} = 2C^M_{sca}$, prevailed when $d^* > d^*_{cr}$ with the critical interparticle distance-to-wavelength ratio d^*_{cr} such that $d^*_{cr} = 2$ for $\chi_s \leq 2$ and $d^*_{cr} = 5$ for $\chi_s > 2$. However, note that these criteria are conservative estimates. In fact, for bispheres with $\chi_s \geq 2$ and different relative index of refraction m, the independent scattering regime was reached for different values of d^* smaller than $d^*_{cr} = 5$.

4.2.2. Effect of m on the asymmetry factor g^b

Fig. 9 presents the asymmetry factor g^b as a function of d^* for bispheres with (a) $\chi_s = 0.063$ or 0.628 and (b) $\chi_s = 2$ or 4 and particle relative index of refraction m varying between 0.667 and 2.6. Here also, the asymmetry factor of bispheres with $\chi_s = 0.063$ was not affected by the relative index of refraction m due to negligible phase shift β across the particles, as previously discussed. However, as observed for $C^b_{sca}/2C^M_{sca}$, the asymmetry factor g^b of bispheres with larger values of χ_s varied with relative index of refraction m due to the non-negligible phase shift β. In addition, Figs. 9(c) and 9(d) plot the ratio g^b/g^M as a function of d^* for bispheres with the same particle size parameters and relative indices of refraction presented in Figs. 9(a) and 9(b), respectively. Fig. 9(d) establishes that for bispheres with $\chi_s \geq 2$ and any relative in-

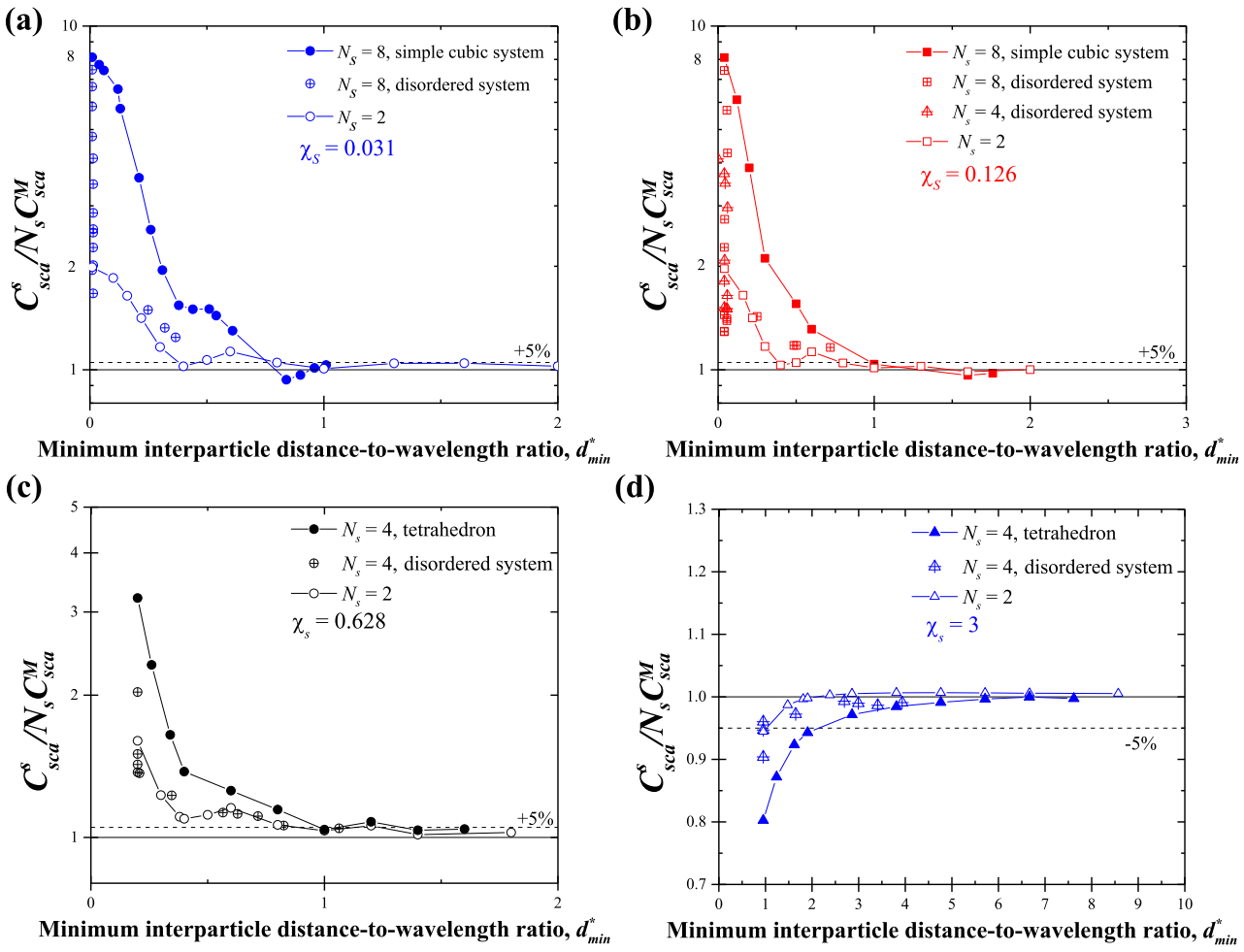

Fig. 10. Scattering cross-section ratio as a function of the minimum interparticle distance-to-wavelength ratio $d^*_{\min}$ for bisphere ($N_s = 2$), ordered, and disordered particle suspensions or aggregates with $N_s = 4$ or 8 for $m = 1.5$ and (a) $\chi_s = 0.031$, (b) $\chi_s = 0.126$, (c) $\chi_s = 0.628$, and (d) $\chi_s = 3$.

dex of refraction m, the transition from dependent to independent scattering occurred for $d^* \geq d^*_{cr} = 2$. On the other hand, for $\chi_s < 2$, d^*_{cr} was larger than 2 for all relative index of refraction m considered [Fig. 9(c)].

Overall, Figs. 8 and 9 indicate that the effect of the relative index of refraction m on dependent effects was negligible for systems with small particle size parameter $\chi_s < 2$, as observed by Olaofe [19] for bispheres and by Ivezić et al. [34] for aggregates. However, the radiation characteristics of bispheres with large particle size parameter $\chi_s \geq 2$ were affected by m. This was in agreement with conclusions made by Ma et al. [35] for aggregates.

4.3. Particle suspensions and aggregates

4.3.1. Scattering cross-section C^s_{sca}

A similar analysis to that previously performed for bispheres was conducted for a 4 particle tetrahedron to identify the parameters governing the scattering characteristics of suspensions and aggregates. The scattering cross-section ratio $C^s_{sca}/N_s C^M_{sca}$ and asymmetry factor g^s of the tetrahedron were found to be also functions of (i) the particle size parameter χ_s, (ii) the relative index of refraction m, and (iii) the interparticle distance-to-wavelength ratio d^* (Figs. S7 and S8 in Supporting Information).

Fig. S9 in Supporting Information plots the scattering cross-section ratio of bispheres, disordered, and ordered particle systems ($N_s = 2$, 4, or 8) as a function of the average interparticle distance-to-wavelength ratio $\bar{d}^*$ with a relative index of refraction $m = 1.5$. First, Fig. S9 indicates that the oscillations for disordered particle suspensions with small particle size parameter χ_s were not as well structured as those obtained for bispheres and ordered particle systems. This was due to variations in the interparticle distance among pairs of particles. Moreover, Fig. S9 shows that ordered particle systems with $N_s = 4$ and 8 featured a critical average interparticle distance-to-wavelength ratio $\bar{d}^*_{cr} = 2$ beyond which independent scattering prevailed for $\chi_s = 0.031$, 0.126, and 0.628 and $\bar{d}^*_{cr} = 5$ for $\chi_s = 3$, as observed for bispheres. However, disordered particle systems featured transition from the dependent to the independent scattering regimes for higher critical average interparticle distance-to-wavelength ratio. In fact, the criterion $\bar{d}^*_{cr} = 2$ developed for bispheres with $\chi_s = 0.031$, 0.126, and 0.628 did not apply to disordered particle systems with the same particle size parameter. This was due to the fact that disordered particle systems had a broader interparticle distance distribution and especially smaller minimum interparticle distances $d_{\min}$ than ordered particle systems (Table S1 in Supporting Information). These observations establish that bispheres were not representative of actual disordered particle suspensions contradicting the hypothesis made by Quirantes et al. [16]. Instead, results for bispheres provided the lower limit for the critical distance d_{cr} among

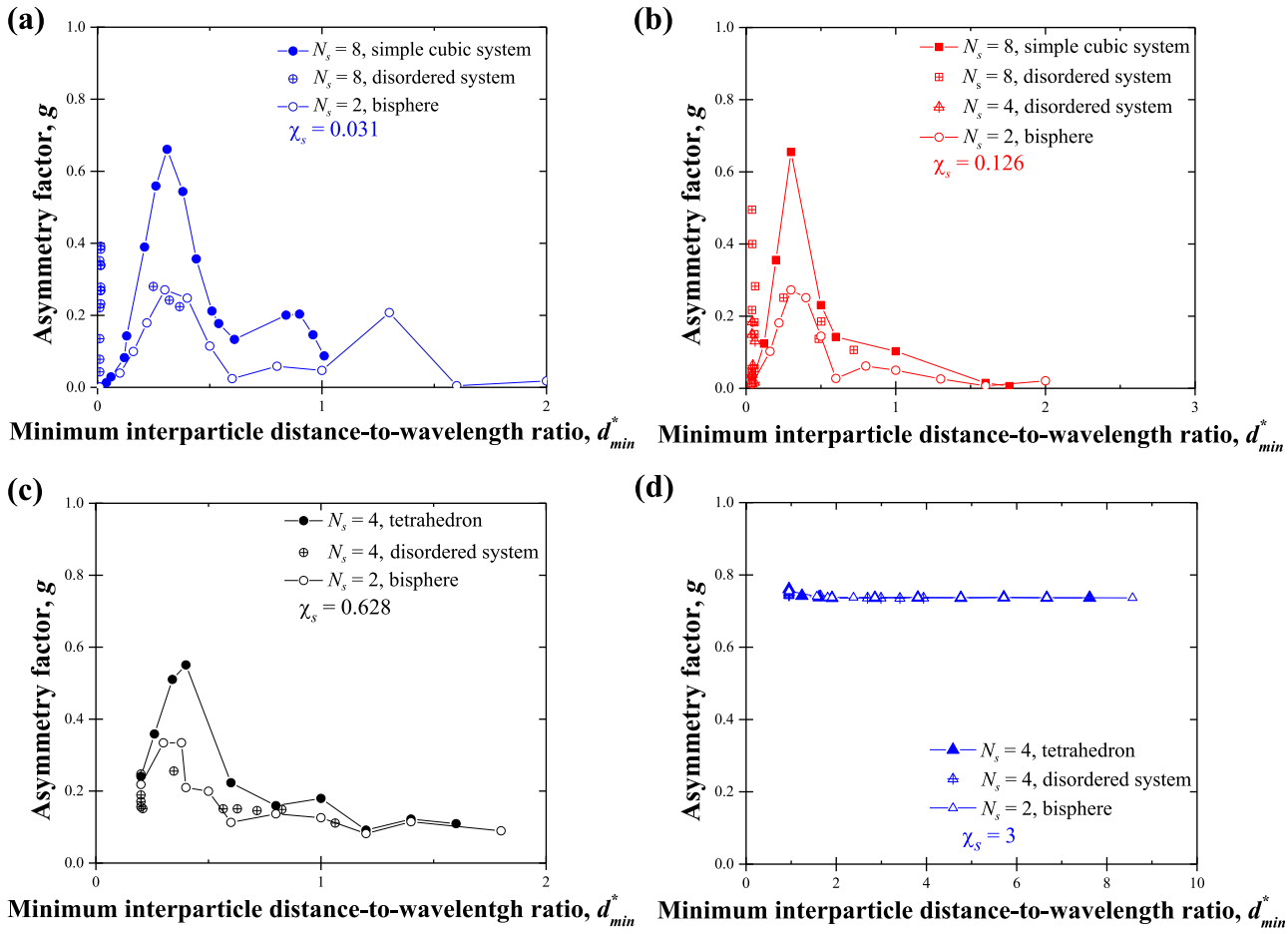

Fig. 11. Asymmetry factor as a function of the minimum interparticle distance-to-wavelength ratio $d^*_{\min}$ for bisphere ($N_s = 2$), ordered, and disordered particle systems with $N_s = 4$ or 8 with $m = 1.5$ and (a) $\chi_s = 0.031$, (b) $\chi_s = 0.126$, (c) $\chi_s = 0.628$, and (d) $\chi_s = 3$.

pairs of particles required to reach the independent scattering regime.

Fig. 10 presents the scattering cross-section of bispheres, disordered, and ordered particle systems ($N_s = 2$, 4, or 8) as a function of the minimum interparticle distance-to-wavelength ratio $d^*_{\min} = d_{\min}/\lambda$ with a relative index of refraction $m = 1.5$. Fig. 10 shows that the criteria (i) $d^*_{min,cr} = 2$ for $\chi_s \leq 2$ and (ii) $d^*_{min,cr} = 5$ for $\chi_s > 2$ developed for bispheres could also be applied conservatively to disordered and ordered particle systems with various interparticle distance distribution. Note that Fig. 10 also indicates that ordered particle systems fell under the independent scattering regime for slightly larger values of $d^*_{\min}$ than that observed for bispheres. This suggests that the total number of particles N_s affected slightly dependent scattering effects.

Figs. S9 and 10 establish that for small particle size parameter $\chi_s = 0.031$, 0.126, and 0.628, (i) dependent effects resulted in $C^s_{sca} \geq N_s C^M_{sca}$ and (ii) the scattering cross-section ratio $C^s_{sca}/N_s C^M_{sca}$ increased with increasing number of particles N_s, as predicted by Eq. (14). These observations were due to the fact that scattering by small particles was isotropic leading to increased multiple scattering with increasing N_s. It is also interesting to note that for simple cubic systems ($N_s = 8$) with small touching spheres such that $\chi_s = 0.031$ and 0.126, $C^s_{sca} = 64 C^M_{sca}$, as predicted by the volume equivalent model [Eq. (14)].

Finally, note that the critical particle volume fraction $f_{v,cr} = 0.006$ proposed by Tien and Drolen [15] and below which independent scattering prevailed for $\chi_s < 0.388$ was found to be inadequate for both the disordered and ordered particle systems simulated in the present study. Indeed, for $\chi_s = 0.031$ and 0.126, the independent scattering regime prevailed for much lower volume fractions (see Fig. S10 of Supporting Information).

4.3.2. Asymmetry factor g^s

Fig. S11 in Supporting Information presents the asymmetry factor g^b and g^s of bispheres, disordered, and ordered particle systems as functions of the average interparticle distance-to-wavelength ratio $\bar{d}^*$. First, Figs. S11(a)-S11(c) show that the asymmetry factor increased with increasing particle number N_s and that oscillations were present for disordered and ordered particle systems for $\chi_s = 0.031$, 0.126, and 0.628. Moreover, Figs. S11(b)-S11(d) indicate that the asymmetry factor of ordered particle systems with $\chi_s \geq 0.1$ and $N_s = 4$ or 8 tended towards those of bispheres ($N_s = 2$) for $\bar{d}^* \geq 2$, unlike that of disordered particle systems. This was due to the broader interparticle distance distribution of disordered systems, as mentioned previously.

Fig. 11 presents the asymmetry factor g^b and g^s of bispheres, disordered, and ordered particle systems as functions of the minimum interparticle distance-to-wavelength ratio $d^*_{\min}$ for the same cases considered in Fig. 10. Fig. 11 shows that the asymmetry factor of disordered and ordered particle systems with $\chi_s \geq 0.1$ converged towards that of bispheres for $d^*_{\min} \geq 2$. Therefore, Fig. 11 suggests that particle suspensions with $\chi_s = 0.628$ and 3 reached the independent scattering regime for the same critical minimum interparticle distance-to-wavelength ratio as bispheres, i.e., when $d^*_{\min} \geq d^*_{min,cr} \simeq 5$. On the other hand, for $\chi_s = 0.031$, Fig. 11 indicates that the independent scattering regime was reached for $d^*_{\min} \geq d^*_{min,cr} > 5$.

5. Conclusion

This study determined (1) the parameters governing the scattering cross-section and asymmetry factor of bispheres, disordered and ordered particle suspensions, and aggregates of non-absorbing spherical particles and (2) the conditions under which dependent and independent scattering regimes prevail for each radiation characteristic. A wide range of parameters was investigated using the DDA method including (i) particle size parameter χ_s varying from 0.031 to 8.05, (ii) relative index of refraction m ranging from 0.667 to 2.6, and (iii) average interparticle distance-to-wavelength ratio $\bar{d}^*$ varying between χ_s/π (touching particles) and 30. The scattering cross-section ratio $C_{sca}/N_s C_{sca}^M$ and asymmetry factor g were shown to be functions exclusively of the number of particles N_s, their size parameter χ_s, their relative index of refraction m, and the interparticle distance-to-wavelength ratio d^*. Additionally, the transition between independent and dependent scattering regimes was shown to be different for the scattering cross-section and the asymmetry factor. For all cases considered, the criteria $\bar{d}^* \geq 2$ for $\chi_s \leq 2$ and $\bar{d}^* \geq 5$ for $\chi_s > 2$ were shown to ensure conservatively that the independent scattering approximation was valid for the scattering cross-section of structures featuring interparticle distances with relatively small standard deviation and for all values of m considered. Similarly, the critical average interparticle distance-to-wavelength ratio $\bar{d}^*_{cr}$ associated with the asymmetry factor (i) reached values as high as 25 for $\chi_s < 2$ and (ii) was equal to $\bar{d}^*_{cr} = 5$ for $\chi_s \geq 2$. Finally, this study demonstrated that results obtained for bispheres could be extended to the disordered particle systems considered provided the transition criteria were based on the minimum interparticle distance-to-wavelength ratio $d^*_{\min}$ instead of on the average interparticle distance-to-wavelength ratio $\bar{d}^*$.

Supporting Information

Scattering cross-section of single spheres computed using the DDA method and the relative error between predictions from the DDA method and the Lorenz-Mie theory as functions of the scattering cross-section predicted by the Lorenz-Mie theory (Figure S1). Asymmetry factor of single spheres computed using the DDA method and the relative error between predictions from the DDA method and the Lorenz-Mie theory as functions of the asymmetry factor predicted by the Lorenz-Mie theory (Figure S2). Scattering cross-section ratio of bispheres with $\chi_s = 0.031$, 0.063, and 1.05 and $m = 1.2$ and/or 2 as a function of the interparticle distance-to-wavelength ratio (Figure S3). Scattering cross-section ratio of bispheres with $\chi_s = 0.031$, 0.063, and 0.126 and $m = 1.5$ as a function of d^*, c^*, c/r_s, and d/r_s (Figure S4). Asymmetry factor of bispheres with $\chi_s = 0.031$, 0.063, and 1.05 and $m = 1.2$ and/or 2 as a function of the interparticle distance-to-wavelength ratio (Figure S5). Asymmetry factor of bispheres with $\chi_s = 0.031$, 0.063, and 0.126 and $m = 1.5$ as a function of d^*, c^*, c/r_s, and d/r_s (Figure S6). Scattering cross-section ratio and asymmetry factor of a tetrahedron ($N_s = 4$) with $\chi_s = 0.063$ and $m = 1.5$ as functions of the interparticle distance-to-wavelength ratio (Figures S7-S8). Scattering cross-section ratio of ordered and disordered systems as a function of the minimum interparticle distance-to-wavelength ratio $d_{\min}$ for $\chi_s = 0.031$, 0.126, 0.628, and 3 (Figure S9). Table with the average interparticle distance and minimum interparticle distance of all the generated particle suspensions and aggregates (Table S1). Scattering cross-section ratio of disordered particle systems with $N_s = 4$ or 8, $m = 1.5$, and $\chi_s = 0.031$, 0.126, 0.628, and 3 as a function of the particle volume fraction f_v (Figure S10). Asymmetry factor of ordered and disordered systems as a function of the minimum interparticle distance-to-wavelength ratio $d_{\min}$ for $\chi_s = 0.031$, 0.126, 0.628, and 3 (Figure S11).

Declaration of Competing Interest

The authors have no competing interest to declare.

CRediT authorship contribution statement

Tiphaine Galy: Conceptualization, Methodology, Formal analysis, Data curation, Visualization, Writing - original draft. **Daniel Huang:** Formal analysis, Data curation, Visualization, Writing - review & editing. **Laurent Pilon:** Conceptualization, Methodology, Formal analysis, Project administration, Supervision, Writing - review & editing.

Acknowledgment

This material is based upon work supported in part by the Advanced Research Projects Agency-Energy (ARPA-E) and its Single-Pane Highly Insulating Efficient Lucid Designs (SHIELD) program (ARPA-E Award No. DE-AR0000738) and the National Science Foundation (NSF) under Grant No. DGE-1735325. This work also used computational and storage services associated with the Hoffman2 Shared Cluster provided by UCLA Institute for Digital Research and Education's Research Technology Group. Tiphaine Galy is grateful to the UCLA Mechanical and Aerospace Engineering Department for financial support through a graduate research fellowship.

Supplementary material

Supplementary material associated with this article can be found, in the online version, at 10.1016/j.jqsrt.2020.106924

References

[1] Wittmaack K. Characterization of carbon nanoparticles in ambient aerosols by scanning electron microscopy and model calculations. J Air Waste Manag Assoc 2004;54(9):1091–8. doi:10.1080/10473289.2004.10470975.
[2] Klenert F, Fruhstorfer J, Aneziris CG, Gross U, Trimis D, Reichenbach I, et al. Microstructure and transmittance of silica gels for application as transparent heat insulation materials. J Solgel Sci Technol 2015;75(3):602–16. doi:10.1007/s10971-015-3731-3.
[3] Kameya Y, Hanamura K. Enhancement of solar radiation absorption using nanoparticle suspension. Sol Energy 2011;85(2):299–307. doi:10.1016/j.solener.2010.11.021.
[4] Park HK, Kim DK, Kim CH. Effect of solvent on titania particle formation and morphology in thermal hydrolysis of ticl4. J Am Ceram Soc 1997;80(3):743–9. doi:10.1111/j.1151-2916.1997.tb02891.x.
[5] Mishchenko MI, Cairns B, Hansen JE, Travis LD, Burg R, Kaufman YJ, et al. Monitoring of aerosol forcing of climate from space: analysis of measurement requirements. J Quant Spectrosc Radiat Transfer 2004;88(1–3):149–61. doi:10.1016/j.jqsrt.2004.03.030.
[6] Mishchenko MI, Mackowski DW, Travis LD. Scattering of light by bispheres with touching and separated components. Appl Opt 1995;34(21):4589–99. doi:10.1364/AO.34.004589.
[7] Nordgaard A, Beckman W. Modelling of flat-plate collectors based on monolithic silica aerogel. Sol Energy 1992;49(5):387–402. doi:10.1016/0038-092X(92)90111-M.
[8] Baetens R, Jelle BP, Gustavsen A. Aerogel insulation for building applications: a state-of-the-art review. Energy Build. 2011;43(4):761–9. doi:10.1016/j.enbuild.2010.12.012.
[9] Zhao L, Yang S, Bhatia B, Strobach E, Wang EN. Modeling silica aerogel optical performance by determining its radiative properties. AIP Adv. 2016;6(2):1–8. doi:10.1063/1.4943215.
[10] Taylor RA, Phelan PE, Otanicar TP, Adrian R, Prasher R. Nanofluid optical property characterization: towards efficient direct absorption solar collectors. Nanoscale Res Lett 2011;6(1):2–11. doi:10.1186/1556-276X-6-225.
[11] Saidur R, Meng T, Said Z, Hasanuzzaman M, Kamyar A. Evaluation of the effect of nanofluid-based absorbers on direct solar collector. Int J Heat Mass Transf 2012;55(21–22):5899–907. doi:10.1016/j.ijheatmasstransfer.2012.05.087.
[12] Auger J-C, Barrera RG, Stout B. Scattering efficiency of clusters composed by aggregated spheres. J Quant Spectrosc Radiat Transfer 2003;79:521–31. doi:10.1016/S0022-4073(02)00305-9.
[13] Diebold MP. Application of light scattering to coatings: auserâs guide. Springer, Berlin, Germany; 2014.
[14] Modest M. Radiative heat transfer. Academic Press, San Diego, CA, USA; 2013.

[15] Tien C-L, Drolen B. Thermal radiation in particulate media with dependent and independent scattering. Ann Rev Heat Transf 1987;1(1):1–32. doi:10.1615/AnnualRevHeatTransfer.v1.30.
[16] Quirantes A, Arroyo F, Quirantes-Ros J. Multiple light scattering by spherical particle systems and its dependence on concentration: a t-matrix study. J Colloid Interface Sci 2001;240(1):78–82. doi:10.1006/jcis.2001.7641.
[17] Kaviany M, Singh BP. Radiative heat transfer in porous media. In: Advances in Heat Transfer, 23. Elsevier; 1993. p. 133–86.
[18] Mishchenko MI, Liu L, Videen G. Conditions of applicability of the single-scattering approximation. Opt Express 2007;15(12):7522–7. doi:10.1364/OE.15.007522.
[19] Olaofe GO. Scattering cross-section for two spheres. Q J Mech Appl Math 1974;27(4):403–22. doi:10.1093/qjmam/27.4.403.
[20] Ivezić Z, Mengüç MP. An investigation of dependent/independent scattering regimes using a discrete dipole approximation. Int J Heat Mass Transf 1996;39(4):811–22. doi:10.1016/0017-9310(95)00142-5.
[21] Bohren C, Huffman D. Absorption and scattering of light by small particles. John Wiley & Sons, New York, NY, USA; 1983.
[22] Daugeron D, Renard J, Personne P, Brun G, André J. Laboratory polarization nephelometer for measurements of optical properties of aerosols. Meas Sci Technol 2007;18(3):632–8. doi:10.1088/0957-0233/18/3/012/meta.
[23] Barkey B, Paulson S, Liou K-N. Polar nephelometers for light scattering by ice crystals and aerosols: design and measurements. In: Kokhanovsky AA, editor. Light Scattering Reviews, 6. Springer, Berlin, Germany; 2012. p. 3–37.
[24] Mishchenko MI. A independent and dependent scattering by particles in a multi-particle group. OSA Continuum 2018;1(1):243–60. doi:10.1364/OSAC.1.000243.
[25] Mishchenko MI, Dlugach JM, Yurkin MA, Bi L, Cairns B, Liu L, et al. First-principles modeling of electromagnetic scattering by discrete and discretely heterogeneous random media. Phys Rep 2016;632:1–75. doi:10.1016/j.physrep.2016.04.002.
[26] van de Hulst HC. Light scattering by small particles. Courier Corporation, North Chelmsford, MA, USA; 1981.
[27] Brewster M, Tien C-L. Radiative transfer in packed fluidized beds: dependent versus independent scattering. ASME J Heat Transf 1982;104(4):573–9. doi:10.1115/1.3245170.
[28] Videen G, Pinnick R, Ngo D, Fu Q, Chỳlek P. Asymmetry parameter and aggregate particles. Appl Opt 1998;37(6):1104–9. doi:10.1364/AO.37.001104.
[29] Tuchin VV, Wang L, Zimnyakov DA. Optical polarization in biomedical applications. Springer Science & Business Media, Berlin, Germany; 2006.
[30] Cartigny J, Yamada Y, Tien C-L. Radiative transfer with dependent scattering by particles: part 1 - theoretical investigation. ASME J Heat Transf 1986;108(3):608–13. doi:10.1115/1.3246979.
[31] Draine B, Flatau P. Discrete-dipole approximation for scattering calculations. J Opt Soc Am A 1994;11(4):1491–9. doi:10.1364/JOSAA.11.001491.
[32] Mackowski DW. A general superposition solution for electromagnetic scattering by multiple spherical domains of optically active media. J Quant Spectrosc Radiat Transf 2014;133:264–70. doi:10.1016/j.jqsrt.2013.08.012.
[33] Mackowski DW, Mishchenko MI. A multiple sphere t-matrix fortran code for use on parallel computer clusters. J Quant Spectrosc Radiat Transf 2011;112(13):2182–92. doi:10.1016/j.jqsrt.2011.02.019.
[34] Ivezić Ž, Mengüç MP, Knauer TG. A procedure to determine the onset of soot agglomeration from multi-wavelength experiments. J Quant Spectrosc Radiat Transf 1997;57(6):859–65. doi:10.1016/S0022-4073(97)00001-0.
[35] Ma L, Tan J, Zhao J, Wang F, Wang C, Wang Y. Dependent scattering and absorption by densely packed discrete spherical particles: effects of complex refractive index. J Quant Spectrosc Radiat Transf 2017;196:94–102. doi:10.1016/j.jqsrt.2017.03.039.
[36] Hottel H, Sarofim A, Dalzell W, Vasalos I. Optical properties of coatings. effect of pigment concentration. AIAA J 1971;9(10):1895–8. doi:10.2514/3.49999.
[37] Churchill SW, Clark GC, Sliepcevich CM. Light-scattering by very dense monodispersions of latex particles. Discuss Faraday Soc 1960;30:192–9. doi:10.1039/DF9603000192.
[38] Harding R, Golding B, Morgen R. Optics of light-scattering films. study of effects of pigment size and concentration. J Opt Soc Am 1960;50(5):446–55. doi:10.1364/JOSA.50.000446.
[39] Ishiniaru A, Kuga Y. Attenuation constant of a coherent field in a dense distribution of particles. J Opt Soc Am 1982;72(10):1317–20. doi:10.1364/JOSA.72.001317.
[40] Yamada Y, Cartigny J, Tien C-L. Radiative transfer with dependent scattering by particles: part 2 - experimental investigation. ASME J Heat Transf 1986;108(3):614–18. doi:10.1115/1.3246980.
[41] Blevin W, Brown W. Effect of particle separation on the reflectance of semi-infinite diffusers. J Opt Soc Am 1961;51(2):129–34. doi:10.1364/JOSA.51.000129.
[42] Jones A. Electromagnetic wave scattering by assemblies of particles in the rayleigh approximation. Proc R Soc Lond A Math Phys Sci 1979;366(1724):111–27. doi:10.1098/rspa.1979.0042.
[43] Draine B., Flatau P.. User guide for the discrete-dipole approximation code DDSCAT 7.3; 2013.